Organic & Biomolecular Chemistry

Accepted Manuscript

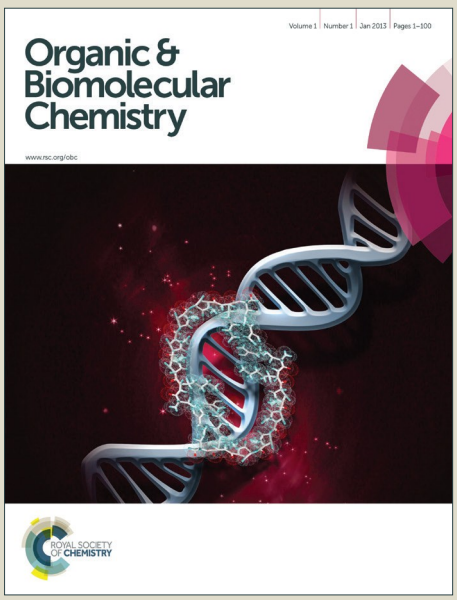

ROYAL SOCIETY OF CHEMISTRY

www.rsc.org/obc

A mechanistic insight into the effect of piperidine as an organocatalyst on the [3+2] cycloaddition reaction of benzalacetone with phenyl azide from a computational study

J. Tajabadi, M. bakavoli*, M. Gholizadeh and H. Eshghi

Department of Chemistry, Faculty of Sciences, Ferdowsi University of Mashhad, Mashhad 91775-1436, Iran.

E-mail: mbakavoli@um.ac.ir; Tel/Fax: +98 5138795457

Several transition structures (TS) for catalyst-free and two plausible mechanistic pathways of the organocatalyzed [3+2] cycloaddition (32CA) between benzalacetone with phenyl azide were located with quantum chemistry methods. Calculations were carried out with B3LYP, MPWB1K and M06-2X functionals using 6-31G(d) and 6-311G(d,p) basis sets at gas and solvent phases. The calculated activation barriers imply that the lowest barrier pathway is the catalyzed process producing **3**-regioisomer through iminium intermediate not dienamine route. Electronic displacements along the reaction path have been examined using a topological analysis of the electron-localization function (ELF). ELF topological analyses along the intrinsic reaction coordinates (IRC) of both catalyzed and uncatalyzed 32CA reactions indicated that while the first C_1-N_1 single bond is formed as a dative bond, the formation of the second C_2-N_3 bond takes place via a C-to-N coupling between the interacting centers of the reagents. Moreover, the ELF analyses imply that the reaction mechanism is the two-stage one-step process in the presence of piperidine organocatalyst, while the bonds formation in uncatalyzed process is almost synchronous.

1 Introduction

1,2,3-Triazoles are useful synthons for transforming into the various medicinally important molecules[1-6]. The widely used approach for construction of these compounds is [3+2] cycloaddition (32CA) reactions. However, classical thermally induced 32CA of azides with alkynes which has been known for over a century[7, 8], owing to the poor regioselectivity (1,4- and 1,5-disubstituted 1,2,3-triazoles), low chemical yield and elevated temperatures required, has not been used much in organic synthesis.

A major breakthrough in the application of the thermally Huisgen cycloaddition reaction is the regiospecific synthesis of isomeric 1,4- and 1,5-disubstituted 1,2,3- triazoles *via* Cu(I)-catalyzed[9, 10] and Ru(II)-catalyzed[11] azide-alkyne cycloaddition reaction, respectively. Other features of the metal catalyzed reactions in comparison to their uncatalyzed counterparts are the high yields accompanied by significant rate acceleration. Despite these remarkable advantages, the toxicity of these metals to

living organisms, metabolic disruption and oxidative DNA degradation are the limiting factors for their widespread applications in bio-material chemistry and chemical biology[12-14].

Metal-free 32CA protocols are also developed to generate triazoles under mild conditions. Bertozzi and co-workers presented a strain-promoted 32CA between cyclooctynes and azides (SPAAC) to form 1,2,3-triazoles for selective modification of biomolecules in vitro and in living cells, with no apparent toxicity[15, 16]. The main disadvantage of SPAAC reaction is the lack of the regioselectivity. An alternative metal-free approach involves the nucleophilic attack of reactive acetylide species to organic azides[17, 18]. In this protocol, only 1,5-diarylsubstituted 1,2,3-triazoles are formed from aryl azides and terminal alkynes in DMSO in the presence of catalytic base.

In recent years, direct access to diversely functionalized 1,2,3-triazoles by applying small organic molecules as organocatalysts has been an exciting research area[19-40]. This methodology has many advantages like high regioselectivity, cheap and readily available starting materials e.g. carbonyl compounds, high yields, access to novel molecules as well as being eco-friendly and the insensitivity of organocatalysts to oxygen and water. These reactions can be categorized upon different reactive intermediates (enamine, dienamine**,** enolate, iminium and etc.) involved in the organocatalytic transformation[26, 36].

In 2015, Wang et al. reported the synthesis of 1,4,5-trisubstituted 1,2,3-triazoles *via* 32CA reaction of α,β-unsaturated ketones with azides in the presence of a piperidine catalyst[41]. They proposed a plausible mechanism to explain the reaction process as shown in Scheme 1. First of all, α,β-unsaturated ketone **1** reacts with piperidine catalyst to form the iminium intermediate **1I**, which can be in equilibrium with dienamine intermediate **1D**. Then 32CA reaction takes place between iminium intermediate **1I** and phenyl azide **2** to form the intermediate **3I**, which releases the catalyst to generate the intermediate **3**. Subsequently, an aerobic oxidation of intermediate **3** generates the final product **P**.

Due to the lacking of theoretical and experimental studies on the mechanism of the mentioned reaction and following our interests in applying the theoretical methods for investigation of the 32CA reactions[42-45], a computational study on the cycloaddition step of the above reaction was performed. In this paper, potential energy surface analysis, conceptual density functional theory (DFT) indices and electron-localization function (ELF) analyses are applied to shed light on the mechanistic details of this reaction.

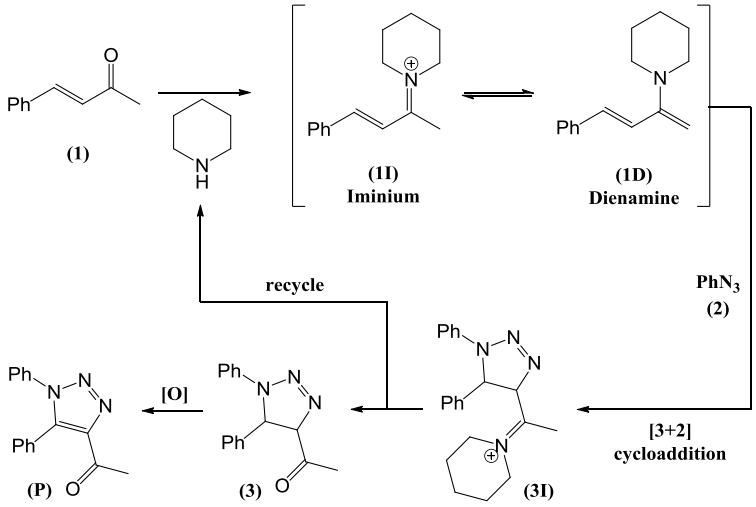

Scheme 1 Proposed mechanism for organocatalyzed 32CA reaction between benzalacetone **(1)** and phenyl azide **(2)**

2 Computational details

All computations were carried out with the Gaussian 09 program suite[46]. Geometries of all species were optimized using the B3LYP[47, 48], MPWB1K[49] and M06-2X[50] functionals with 6-31G(d) basis set. Solvent effects of dimethylsulfoxide (DMSO) and toluene were taken into account by single-point calculations of the gas phase structures using the conductor-like polarisable continuum model[51, 52] in the framework of the self-consistent reaction field, CPCM-SCRF, with 6-311G(d,p) basis set. An ultrafine grid was used with the M06-2X geometry optimization and frequency calculations. The stationary points were characterized by vibrational frequency calculations in order to verify that the reactants and products have positive definite Hessian matrices and the TSs had one and only one imaginary frequency. The vibrational mode was assigned appropriately by means of the visual inspection and animation. In all calculations in the gas phase, the ideal gas approximation, at the standard conditions were assumed. The intrinsic reaction coordinate (IRC) calculations were performed on the TSs to determine the connectivity of the TS structure to the corresponding products and reactants using the second-order Gonzalez–Schlegel integration method[53, 54]. Topological analysis of ELF was carried out with the TopMod suite[55]. All molecular graphics was generated using the GaussView 05 software[56].

3 Results and discussion

For investigation of the mechanistic aspects of uncatalyzed and organocatalized 32CA reaction between the benzalacetone and phenyl azide, a computational analysis was performed and the results have been presented in three sections. In the first section, energetic aspects and geometrical parameters of the TSs will be discussed. In the second section, an analysis of the DFT

reactivity indices at the ground state of the reagents is given. Finally, the results from an exhaustive analysis of the topology of the ELF will be presented and discussed at the last section.

3.1 Mechanism studies

As mentioned above, the reaction between α,β-unsaturated ketone **1** with piperidine catalyst gives either iminium ion (**1I**) or dienamine (**1D**) intermediates. **1**, **1I** and **1D** have two isomers of s-cis (**c**) and (or) s-trans (**t**) (Scheme 2), which can react with phenyl azide **2**. The Gibbs energy differences between s-cis and s-trans forms ($G_{s\text{-}cis}$-$G_{s\text{-}trans}$) of **1**, **1I** and **1D** are -1.4, 3.6 and 0.4 kcal mol^{-1}, respectively, at the MPWB1K/6-311G(d,p)//MPWB1K/6-31G(d) level. Two regioisomeric pathways are possible for each of the geometric isomers leading to cycloadducts in which terminal nitrogen of azide is either bonded to α–carbon (**3** regioisomer) or β–carbon (**4** regioisomer) of the unsaturated dipolarophile. For each of regioisomeric pathways, phenyl azide can approach the dipolarophiles in two directions at the TSs. If the phenyl group of dipole and substituents on C_1 or C_2 carbon atoms of dipolarophiles are oriented in the same direction, it is identified as *endo* (**n**) and for the opposite direction as *exo* (**x**). Moreover, in the catalyzed reactions, two faces of dipolarophiles, *re*-face (**r**) and *si*-face (**s**), are not quite equal; hence there are two possible paths for approaching of dipole to dipolarophiles at the TSs. Therefore, eight and sixteen TSs are possible for uncatalyzed and catalyzed processes, respectively. Through these TSs, the related minima associated with the cycloadducts can be obtained. It is worth noting that the same cycloadducts are obtained from the TSs with *endo* and *exo* orientations (Scheme 2).

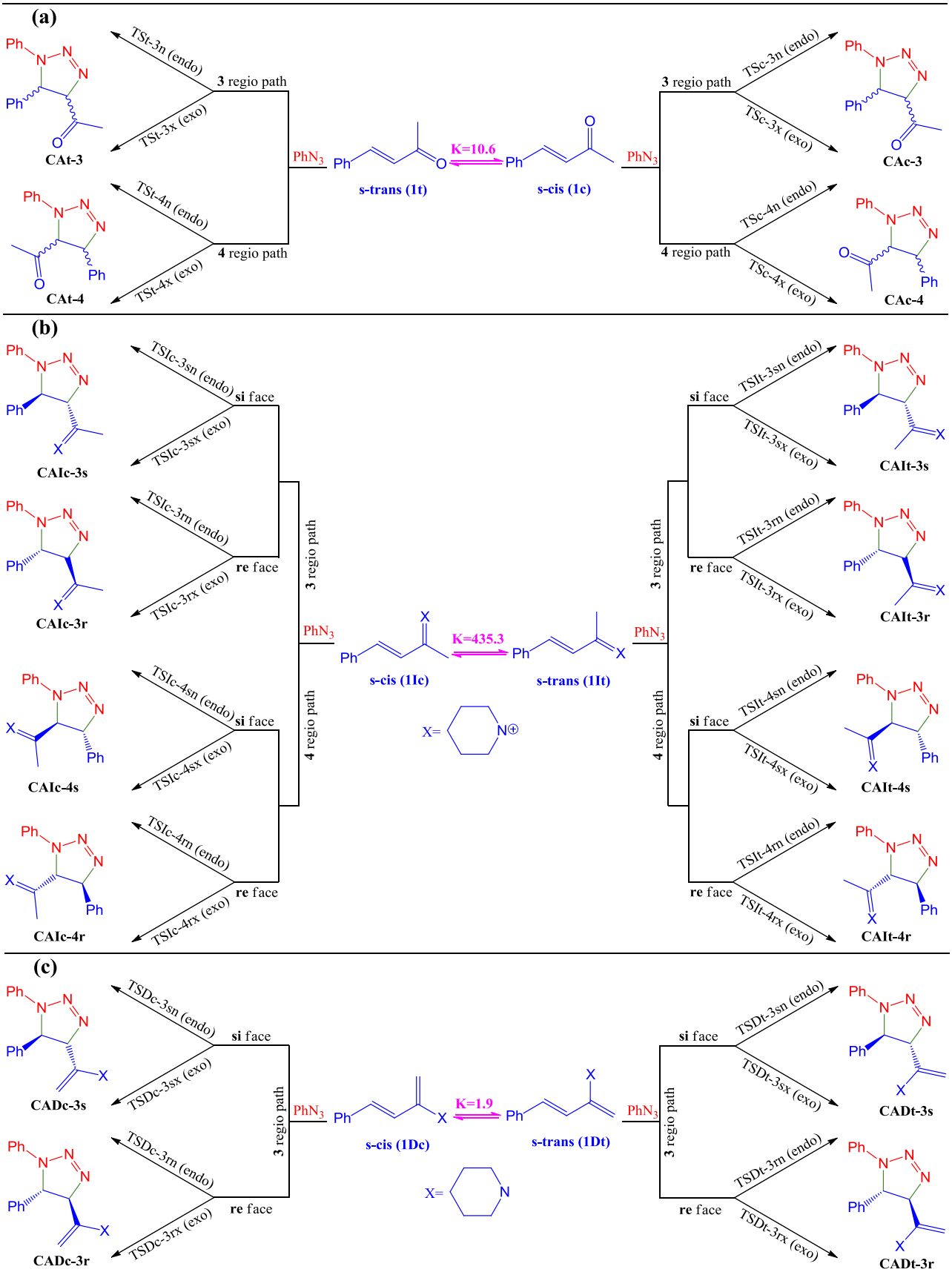

Scheme 2 A schematic representation of all stationary points along the: (a) catalyst-free process, (b) catalyzed reaction through iminium intermediate and (c) catalyzed reaction through dienamine intermediate associated with the observed **3**-regioisomers

All the possible TSs were located for uncatalyzed process (eight pathways) and catalyzed reaction through iminium intermediate (sixteen pathways). Moreover, for the reaction through dienamine intermediate, only eight TSs were located associated with the observed regioisomers (**3**-regioisomers). The potential energy diagram and geometries of the TSs, corresponding to the most favorable pathways of these processes have been illustrated in Fig. 1 and Fig. 2, respectively.

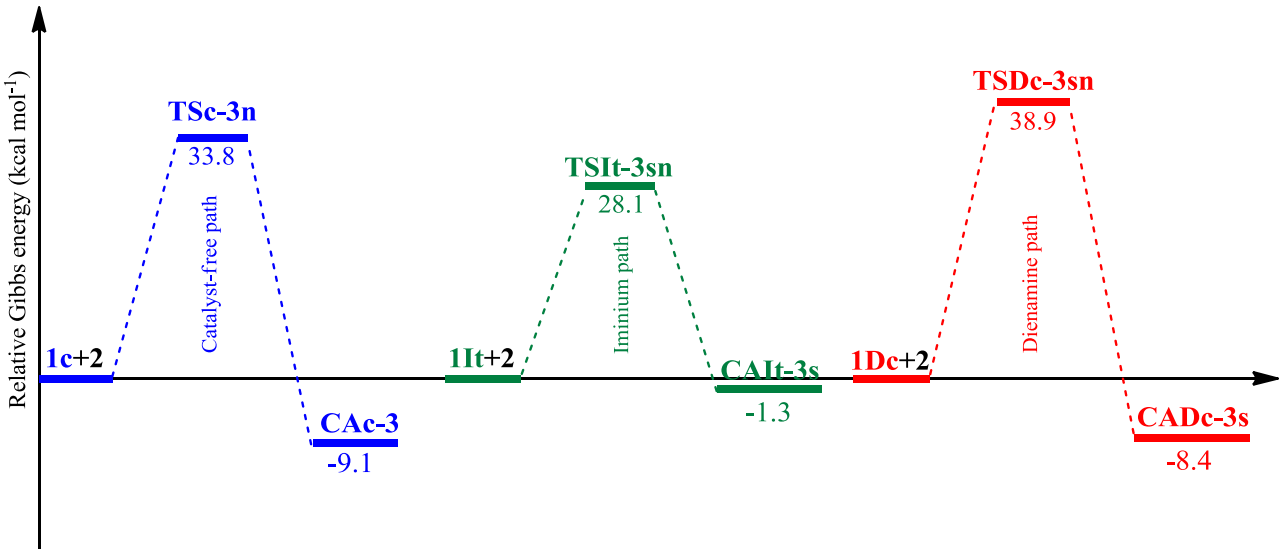

Fig. 1 Computed potential energy diagram for the most favorable pathways in the catalyst-free and organocatalized 32CA reactions between phenyl azide **2** as dipole and **1c**, **1It** and **1Dc** as dipolarophiles. Energies are given in kcal mol^{-1}. All data have been computed at the MPWB1K/6-311G(d,p)//MPWB1K/6-31G(d) level.

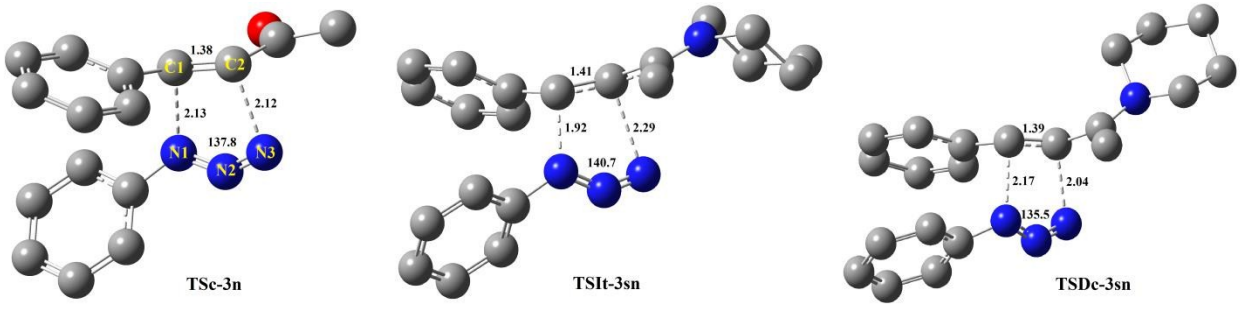

Fig. 2 The most favorable TSs at the MPWB1K/6-31G(d) level in the catalyst-free (**TSc-3n**), catalyzed through iminium intermediate (**TSIt-3sn**) and catalyzed through dienamine intermediate (**TSDc-3sn**) processes. Bond lengths are given in Angstrom.

Table 1. Calculated relative activation and thermodynamic parameters, in kcal mol^{-1}, at the MPWB1K/6-311G(d,p)//MPWB1K/6-31G(d) level[a]

		Gas phase				Toluene				DMSO			
	Structures	**$\Delta G^{\ddagger}$[b]**	**ΔG^{c}_{rxn}**	**$\Delta H^{\ddagger}$**	**ΔH_{rxn}**	**$\Delta G^{\ddagger}$**	**ΔG_{rxn}**	**$\Delta H^{\ddagger}$**	**ΔH_{rxn}**	**$\Delta G^{\ddagger}$**	**ΔG_{rxn}**	**$\Delta H^{\ddagger}$**	**ΔH_{rxn}**
Catalyst-free path	**TSc-3n**	33.8	-9.1	20.0	-25.0	34.2	-8.2	20.4	-24.1	34.5	-7.4	20.8	-23.2
	TSt-3n	37.2	-10.6	21.5	-25.8	37.8	-9.5	22.1	-24.7	38.1	-8.5	22.4	-23.7
	TSc-3x	34.4	-9.1	19.6	-25.0	35.6	-8.2	20.8	-24.1	36.5	-7.4	21.8	-23.2
	TSt-3x	36.8	-10.6	22.1	-25.8	37.1	-9.5	22.5	-24.7	37.4	-8.5	22.8	-23.7
	TSc-4n	36.9	-5.1	22.5	-20.1	37.8	-5.8	23.4	-20.8	38.4	-6.5	24.0	-21.5
	TSt-4n[d]												
	TSc-4x	37.8	-5.1	23.4	-20.1	38.4	-5.8	24.0	-20.8	38.7	-6.5	24.3	-21.5
	TSt-4x	35.0	-8.5	21.2	-23.7	36.1	-7.5	22.3	-22.6	37.0	-6.5	23.2	-21.6
Iminium path	**TSIt-3rn**	29.0	-1.1	15.0	-16.0	32.3	-1.9	18.2	-16.7	34.6	-2.8	20.5	-17.6
	TSIt-3sn	28.1	-1.3	14.3	-16.7	31.3	-1.1	17.4	-16.5	33.5	-1.4	19.7	-16.8
	TSIt-3rx	28.9	-1.1	15.4	-16.0	32.3	-1.9	18.8	-16.7	34.9	-2.8	21.3	-17.6
	TSIt-3sx	30.3	-1.3	14.9	-16.7	33.8	-1.1	18.5	-16.5	36.4	-1.4	21.1	-16.8
	TSIc-3rn	30.4	-1.2	16.2	-17.8	33.4	-1.5	19.2	-18.1	35.5	-2.0	21.4	-18.6
	TSIc-3sn	32.1	-3.5	18.6	-18.3	35.4	-3.3	21.8	-18.1	37.7	-3.6	24.1	-18.4
	TSIc-3rx	30.1	-1.2	16.7	-17.8	33.5	-1.5	20.1	-18.1	36.0	-2.0	22.6	-18.6
	TSIc-3sx	31.2	-3.5	16.8	-18.3	34.6	-3.3	20.2	-18.1	37.1	-3.6	22.7	-18.4
	TSIt-4rn	36.9	-0.3	21.7	-15.0	38.7	-1.5	23.5	-16.2	39.7	-2.9	24.5	-17.6
	TSIt-4sn	38.7	0.1	22.3	-15.1	40.3	-0.7	23.9	-16.0	41.2	-1.9	24.8	-17.1
	TSIt-4rx	36.8	-0.3	21.9	-15.0	38.7	-1.5	23.8	-16.2	39.8	-2.9	25.0	-17.6
	TSIt-4sx	37.4	0.1	22.1	-15.1	39.4	-0.7	24.0	-16.0	40.5	-1.9	25.2	-17.1
	TSIc-4rn	38.1	-1.5	23.0	-15.3	40.0	-2.2	24.9	-16.1	41.1	-3.3	26.0	-17.1
	TSIc-4sn	39.1	-1.5	23.8	-16.4	40.8	-1.9	25.6	-16.9	41.9	-2.8	26.6	-17.7
	TSIc-4rx	36.1	-1.5	22.0	-15.3	38.2	-2.2	24.2	-16.1	39.6	-3.3	25.5	-17.1
	TSIc-4sx	36.7	-1.5	22.2	-16.4	38.7	-1.9	24.3	-16.9	40.0	-2.8	25.6	-17.7
Dienamine path	**TSDc-3sn**	38.9	-8.4	22.6	-22.9	39.5	-8.8	23.2	-23.3	39.8	-9.3	23.5	-23.8
	TSDt-3sn	40.1	-7.5	24.8	-22.9	40.7	-7.5	25.5	-22.9	41.1	-7.6	25.9	-23.0
	TSDc-3sx	41.5	-8.4	26.8	-22.9	42.0	-8.8	27.3	-23.3	42.4	-9.3	27.7	-23.8
	TSDt-3sx	40.2	-7.5	25.6	-22.9	40.8	-7.5	26.2	-22.9	41.3	-7.6	26.7	-23.0
	TSDc-3rn	39.6	-7.6	23.6	-22.6	40.2	-7.7	24.2	-22.7	40.5	-7.8	24.6	-22.9
	TSDt-3rn	40.1	-7.1	23.9	-22.6	40.7	-7.2	24.5	-22.6	41.1	-7.3	24.9	-22.7
	TSDc-3rx	39.1	-7.6	24.2	-22.6	39.6	-7.7	24.8	-22.7	40.0	-7.8	25.2	-22.9
	TSDt-3rx	39.4	-7.1	24.7	-22.6	39.8	-7.2	25.2	-22.6	40.1	-7.3	25.5	-22.7

[a] The MPWB1K/6-31G(d) Gibbs energy and enthalpy corrections have been added to the MPWB1K /6-311G(d,p) single-point energies.

[b] $\Delta G^{\ddagger} = G(\mathrm{TS}) - G(\mathrm{dipole}) - G(\mathrm{dipolarophile})$.

[c] $\Delta G_{rxn} = G(\mathrm{product}) - G(\mathrm{dipole}) - G(\mathrm{dipolarophile})$.

[d] This TS was not founded.

At first, all stationary points were optimized at the B3LYP/6-31G(d) level. The B3LYP hybrid density functional enjoys a vast popularity in the chemistry community, but there is the increasing alarming reports concerning large errors in energetics[57-60]. Zhao and Truhlar recommended the MPWB1K and M06-2X functionals for main-group thermochemistry and kinetics[49, 50, 61]. M06-2X has been shown to be outstanding to capture stacking effects[62], which can be present in the TSs studied. MPWB1K has also shown to have good results in processes including weak interactions[49]. Moreover, it has been shown that MPWB1K and M06-2X are of the best methods of predicting reaction enthalpies and activation barriers for cycloadditions[57, 63,64]. Therefore, all

stationary points were reoptimized at the MPWB1K/6-31G(d) and M06-2X/6-31G(d) levels and also single-point energy calculations using 6-311G(d,p) basis set on these optimized geometries were performed. Solvent effects of DMSO and toluene were taken into account by single-point calculations of the gas phase structures using the CPCM-SCRF, with 6-311G(d,p) basis set. Calculated relative thermodynamic and activation parameters of the reactions in the gas phase, DMSO and toluene at the MPWB1K/6-311G(d,p)//MPWB1K/6-31G(d) level have been reported in Table 1. These parameters at the other levels are presented in Supporting Information. A brief discussion about comparison of these functionals and basis sets is presented in the Supporting Information. In the following discussion we will refer to the MPWB1K/6-311G(d,p)//MPWB1K/6-31G(d) Gibbs energy results otherwise noted.

A comparison of the activation energies presented in Table 1 indicates that the catalyzed reactions through iminium and dienamine intermediates are faster and slower compared to uncatalyzed reaction, respectively. While α,β-unsaturated ketone **1c** and phenyl azide **2** requires 33.8 kcal mol^{-1} Gibbs energy to achieve the corresponding TS (**TSc-3n**) in the gas phase, this value is 28.1 kcal mol^{-1} for iminium **1It** (**TSIt-3sn**) and 38.9 kcal mol^{-1} for dienamine **1Dc (TSDc-3sn**). The difference in the activation energy of two plausible intermediates in the catalyzed mechanism is 10.8 kcal mol^{-1}; therefore, the catalytic reaction proceeding through the dienamine intermediate can be ruled out. Here after, our purpose of catalyzed reaction is the reaction through iminium intermediate. The piperidine organocatalyst has significant effects on the reactivity and selectivity of the reaction. It reduces the activation energy of this process by 5.7 kcal mol^{-1}, hence, the rate constant of the catalyzed process is 1.51×10^{4} more than uncatalyzed one at 298.15 K. Moreover, it affects the regioisomeric ratio. The difference in activation energy between the most favorable TSs in **3**- and **4**-regioisomeric pathways is 1.2 and 8.0 kcal mol^{-1} for the uncatalyzed and catalyzed reactions, respectively. Therefore, organocatalyst allows the **3**-regioisomers to be produced solely in clear agreement with experimental findings[41]. It is worth noting that the M06-2X results show that in all **3**-regioisomeric pathways, the *endo* orientation of phenyl groups on the dipole and dipolarophile is slightly favorable compared to the *exo* orientation; however, this is not observed from MPWB1K results. It is presumably due to stacking effects of two phenyl groups of the endo orientation that M06-2X has been shown to be outstanding to capture them[62].

Calculated thermodynamic parameters indicates that all possible pathways are exothermic (except two pathways), in the range of 0.1 to -10.6 kcal mol^{-1} and the **3**-regioisomers are slightly more stable than **4**-regioisomers, thermodynamically. The exothermicity of the uncatalyzed reaction is 7.8 kcal mol^{-1} more than catalyzed ones.

When the solvent effects of DMSO and toluene are included, the reaction exothermicities increased slightly in the most pathways. The changes are in the range of 0.1-2.6 and 0.0-1.1 kcal mol^{-1} for DMSO and toluene solvents, respectively. On the other hand, the solvent effects increase the activation energies by a higher solvation of the reagents than TSs in all pathways,

especially in the catalyzed process through iminium intermediate that has an ionic nature. DMSO solvent increases the activation energies in the range of 0.6-2.1, 2.5-6.2 and 0.8-1.1 kcal mol^{-1} for catalyst-free and catalyzed processes through iminium and dienamine intermediates, respectively. These increments are in the range of 0.4-1.2, 1.8-3.5 and 0.5-0.6 kcal mol^{-1} in the toluene. The activation energies for **TSc-3n**, **TSIt-3sn** and **TSDc-3sn** in DMSO are 0.7, 5.4 and 0.9 kcal mol^{-1} as well as in toluene are 0.4, 3.2 and 0.6 kcal mol^{-1} higher than gas phase, respectively. Therefore, a polar DMSO solvent decreased the rate of this reaction greater than non-polar toluene solvent. Consequently, the activation energy difference between uncatalyzed and catalyzed processes decreased from 5.7 kcal mol^{-1} in the gas phase to 1.0 and 2.9 kcal mol^{-1} in the DMSO and toluene, respectively.

3.2 Analysis of the DFT reactivity indices of the reactants

The global DFT reactivity indices of the reactants at B3LYP/6-31G(d) level have been provided in Table S4. The electronic chemical potential of the phenyl azide **2** is slightly higher and lower than that of the dipolarophiles **1** and **1D**, respectively. Organocatalyst causes a significant decrease (3.81 eV) in the chemical potential of dipolarophile **1**. The electronic chemical potential of dipole **2** (-3.62 eV), is higher than those of the cationic dipolarophile **1It** (-7.92 eV). Therefore, it can be concluded while the flux of electron density should goes from **2** to **1 and 1It**, an inversion of the flux of electron density is occurred in the case of **2** and **1D**, which goes from **1D** to **2**.

According to the absolute scale of electrophilicity[65] and nucleophilicity[66] based on ω and N index, dipole **2** can be classified as moderate electrophile with ω indices of 1.27 eV and moderate nucleophile with N indices of 2.92 eV. On the other hand, while catalyst-free dipolarophile **1** is a strong electrophile (ω = 1.89 eV) and moderate nucleophile (N = 2.77 eV), **1D** is vice versa; i.e. it is a moderate electrophile (ω = 1.22 eV) and strong nucleophile (N = 3.81 eV). Moreover, the piperidine organocatalyst causes a significant change in the electrophilicity and nucleophilicity of dipolarophile **1** in the iminium form **1I**. The formation of a cationic intermediate lowers the HOMO and LUMO energy levels considerably, which increases the electrophilicity and decreases the nucleophilicity indices, greatly. Interestingly, the nucleophilicity of **1It** is -0.61 eV, which is lower than tetracyanoethylene (TCE), 0.00 eV, as the weakest nucleophile in a large series of molecules already investigated in the context of polar cycloaddition reactions[67]. On the other hand, the electrophilicity of **1It** is 8.64 eV and it is only 0.33 eV lower than N-methylmethyleneammonium cation as the strongest electrophile[65]. Electrophilicity difference of dipole/dipolarophile pairs ($\Delta\omega$) proposed as a useful tool to indicate the polarity of cycloaddition reactions[65]. The electrophilicity differences of dipole **2** and dipolarophiles **1c**, **1Dt** and **1It** are 0.62, 0.05 and 7.37 eV, respectively; indicating a non-polar character for the reaction of dipole **2** with **1c** and **1Dt** and a polar character for **1It**. This large increase in $\Delta\omega$ for the organocatalized iminium mediated reaction accounts for the acceleration of the cycloaddition.

The polar nature of these reactions was also evaluated by computing the global electron density transfer (GEDT)[68] at the TSs. The natural atomic charges at the TSs were obtained through a natural population analysis (NPA)[69, 70] using the M06-2X/6-31G(d) levels of the theory. The values of the GEDT fluxing from the phenyl azide framework to the dipolarophiles are given in Table S2. The GEDT between phenyl azide **2** and ketones **1** as well as **1D** at the corresponding TSs is negligible (-0.05 to 0.05 e which negative values indicate an inversion of the flux of the electron density) in good agreement with very low electrophilicity differences, indicating a non-polar character for these reactions. On the other hand, the GEDT values between the phenyl azide **2** and **1It** at different possible TSs are in the range of 0.08 – 0.23 e, imply that this process has a polar character. These medium GETDs could be due to moderate nucleophilicity of phenyl azide. It is reasonable to suppose a correlation between the polar characters of these reactions, measured by the GEDT at the corresponding TS, and the activation energy. As the GEDT values at the catalyzed TSs increases, the activation energies decreases and enhance the reaction rate. This correlation has been observed in Diels–Alder[71, 72] and *ene*[73] reactions, previously. In catalyzed process, the values of GEDT at the **3**-regioisomeric TSs (0.17 - 0.23 e) are greater than **4**-regioisomeric ones (0.08 – 0.11 e) in good correlation with low activation energy of the formers. It should be noted that there is not a good correlation between the activation energies and GEDT values of the different TSs in **3**-regioisomeric path. For instance, while the activation energy of the **TSIt-3sn** is less than other **3**-regioisomer TSs, the GEDT value at this TS is less than the others.

Recently, local Parr functions were proposed for the prediction of the regioselectivity based on DFT reactivity indices of the reactants in polar organic reactions[74]. The electrophilic, P_k^+, and nucleophilic, P_k^-, Parr functions were computed at different levels based on the Mulliken spin density distribution at the radical anion of dipolarophile **1It** and the radical cation of dipole **2**. The calculated results at the reactive centers have been listed in Table S5. It is correctly predicted that the β–carbon of dipolarophile **1It** is a more electrophilic center than α–carbon at all levels; while the prediction of more nucleophilic nitrogen of phenyl azide depends on the employed basis set. Using the 6-31G(d), 6-31+G(d) and 6-311G(d,p) basis sets, B3LYP, MPWB1K and M06-2X functionals predict a more nucleophilic center for terminal nitrogen of azide or the same nucleophilicity for two reactive nitrogen of azide which is in disagreement with the experimental data. On the other hand, all three functionals, by using a larger 6-311+G(d,p) basis set, provide a correct prediction of more nucleophilic center of phenyl azide, i.e. N_1 atom. The electrophilic Parr function, P_k^+, for the C_1 and C_2 carbon atoms of **1It** and the nucleophilic Parr function, P_k^-, for the N_1 and N_3 nitrogen atoms of phenyl azide were depicted in Fig. 3.

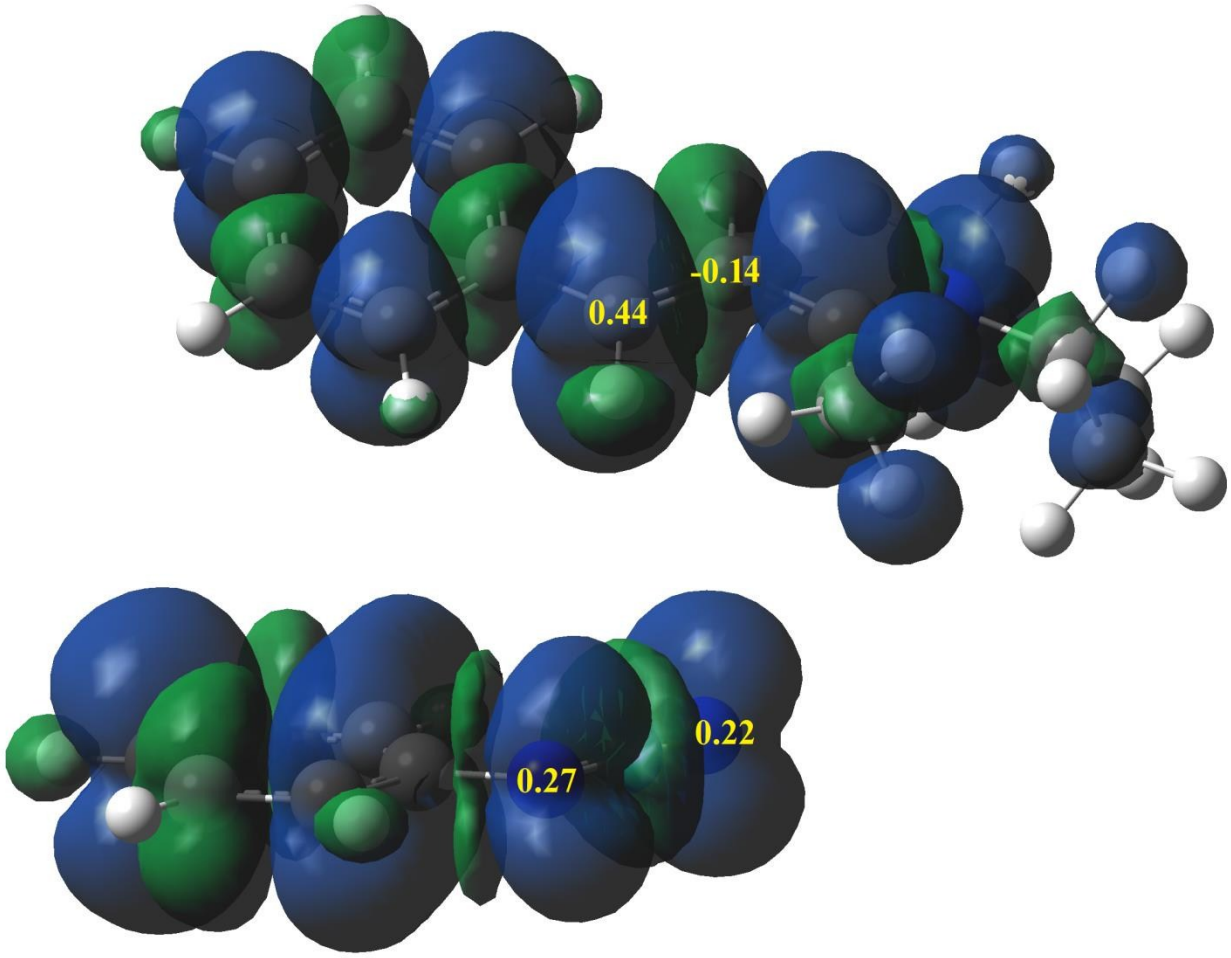

Fig. 3 The atomic spin density maps of the radical cation of phenyl azide and the radical anion of **1It** at the M06-2X/6-311+G(d,p)//M06-2X/6-31G(d) level.

3.3 ELF topological analysis along the reaction coordinates

The population analysis performed within the ELF basins has been found to be a useful tool to clarify the changes in bonding that occurs along the reaction coordinate[75-80]. In order to obtain additional information for the electron density evolution in these reactions, an ELF topological analysis of the M06-2X/6-31G(d) wave functions was performed along the IRC profile associated with the most favorable TSs of the uncatalyzed (**TSc-3n**) and catalyzed (**TSIt-3sn**) processes. The calculated reaction path comprises a total of 160 points with a step size of 0.05 amu$^{1/2}$ Bohr. The ELF topology evolutions along the reaction paths involve eleven and twelve structural stability domains connected by turning points for the uncatalyzed and catalyzed processes, respectively. The population, *N*, of the most relevant basins at the turning points were listed in Tables S7 and S8. For completeness, the ELF analyses of the isolated reactants and products as well as the initial point calculated on the IRC path are included. The attractor positions and atom numbering for the most relevant points were shown in Figs. 4, S1 and S2. Details of

these ELF topological analyses are also given in the Supporting Information. Herein, some appealing conclusions can be drawn from the ELF analysis are presented.

3.3.1 Isolated reactants. Some appealing conclusions can be drawn from the ELF analysis of the isolated phenyl azide **2** and dipolarophiles **1c** and **1It** (see Supporting Information): i) structure of phenyl azide **2** is a hybrid resonance of **2a-c** and the diradical structure **2d** can be rejected due to the lack of monosynaptic basin associated with the lone pair on the middle nitrogen atom (see Scheme 3, Fig. 4 and Table S6); ii) **1It** has slightly more resonance in its π conjugated framework relative to **1c**.

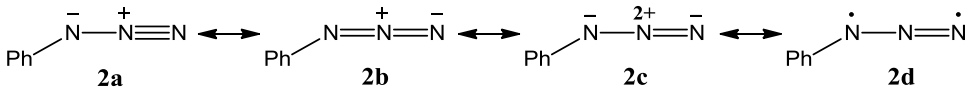

Scheme 3 Proposed resonance structures of the phenyl azide **2**

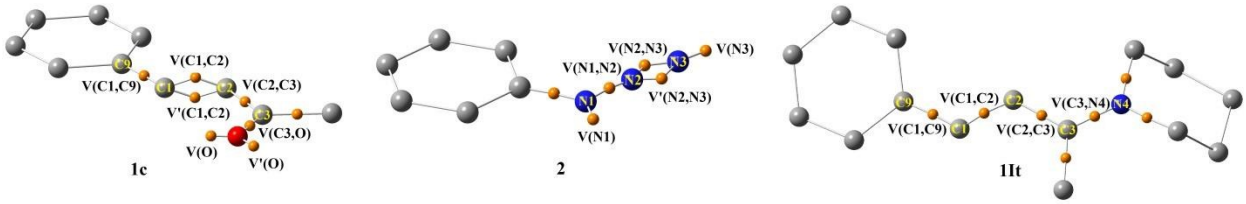

Fig. 4 ELF attractor positions and atom numbering for the most relevant points associated with the isolated reactants **2**, **1c** and **1It**

*3.3.2 Catalyst-free process associated with the 32CA reaction between α,β-unsaturated ketone **1c** and phenyl azid **2**.* Some appealing conclusions can be drawn from the ELF analysis of the 32CA reaction between α,β-unsaturated ketone **1c** and phenyl azid **2** (see Supporting Information): i) the most important change on the electron density of the reactants before reaching the TS is the creation of a $V(N_2)$ monosynaptic basin associated with the lone pair of the middle nitrogen of phenyl azide **2** as a consequence of depopulation of the $V(N_1,N_2)$ and $V(N_2,N_3)$ disynaptic basins. Its initial population is 0.52e and reached to 2.14e at the TS; ii) after the TS, the C_2 carbon atom on the dipolarophile **1c** has acquired the *pseudoradical*[81, 82] character in a very early point ($d(C_2\text{-}N_3$=2.079 Å)) compared with point where C_2-N_3 single bond begins to form ($d(C_2\text{-}N_3$=1.714 Å)); iii) formation of the C_1-N_1 single bond begins at a distance of 1.901 Å by the donation of the electron density of the non-bonding lone pair present at the N_1 nitrogen of dipole **2** to the β-conjugated C_1 carbon of dipolarophile **1c**, with an initial population of 1.34e. It is worth noting that the C_1 carbon of **1c** is the most electrophilic center of this species; iv) at $d(C_2\text{-}N_3)$=1.714 Å, two monosynaptic basins, $V(C_2)$ correspond to the *pseudoradical* C_2 carbon created at **1c** in early point and $V'(N_3)$ as a result of dividing of non-bonding lone pair present at the N_3 nitrogen of dipole **2**, collapse into a new disynaptic basin $V(C_2\text{-}N_3)$ results in the second bond formation and ring closure, with an initial population of 1.32e; v) the populations of two new formed C-N bonds in the

product, 1.66e and 1.73e, are less than a typical single C-C bond possessing a population of 1.9-2.1e, due to the presence of an electronegative nitrogen atom that attracts the electron density of the bond basin.

3.3.3 organocatalyzed process. Some appealing conclusions can be drawn from the ELF analysis of the 32CA reaction between **1It** and phenyl azid **2** (see Supporting Information): i) the most important change on the electron density of the reactants before reaching the TS that similar to catalyst-free process, is the creation of a $V(N_2)$ monosynaptic basin associated with the non-bonding lone pair of the middle nitrogen of phenyl azide **2**, with a population of 0.62e and 2.05e at first and the TS, respectively; ii) at the TS, two monosynaptic basins are created on the C_1 and C_2 carbon atoms of dipolarophile **1It**, simultaneously, possessing different populations (N[$V(C_1)$]=0.06e and N[$V(C_2)$]=0.22e). The new monosynaptic basin on the C_1 carbon as the most electrophilic center of **1It**, similar to α,β-unsaturated ketone **1c**, has a very short life and disappeared very fast; however, the population of $V(C_2)$ increases slowly along the reaction path until the creation of C_2-N_3 single bond at the last stage; iii) formation of the first bond is between the most electrophilic center of the dipolarophile **1It** (C_1) and the most nucleophilic center of the dipole **2** (N_1) at the distance of 1.854 Å by the donation of the electron density of the non-bonding lone pair on the N_1 nitrogen to the C_1 carbon, with an initial population of 1.37e. At this point, there is no monosynaptic basin on the N_3 atom of dipole **2**, which will be created in a further step of the IRC and precedes the creation of the disynaptic basin $V(C_2,N_3)$. These behaviors assert the two-stage one-step[83] nature of the process, where the C_2-N_3 bond is formed in the final step of the IRC, after completion of the C_1-N_1 bond formation; iv) formation of the second C_2-N_3 single bond begins at the 1.748 Å by sharing the electron density of the non-bonding lone pair present at the N_3 nitrogen of dipole **2** ($V'(N_3)$), as a consequence of the split of the $V(N_3)$, and that of the *pseudoradical* C_2 carbon created at **1It**, with an initial population of 1.16e; v) as two fragments are approached together, the GEDT that fluxes from the phenyl azide **2** toward iminium ion **1It** increases so far it reaches to maximum amount at TS (0.17e). Afterward, the GEDT decreases continuously, so far it fluxed in a reverse direction from the dipolarophile **1It** toward the dipole **2**.

4. Conclusion

A computational study was carried out with B3LYP, MPWB1K and M06-2X functionals using the 6-31G(d) and 6-311G(d,p) basis sets for investigation of the mechanistic aspects of the catalyst-free and organocatalized 32CA reaction between the benzalacetone **1** and phenyl azide **2**. The most important points are: (1) Based on activation energies, the catalyzed reactions through the iminium and dienamine intermediates are faster and slower compared to uncatalyzed reactions, respectively. Therefore, the mechanism through dienamine catalysis is ruled out. Moreover, the organocatalyst increases the regioselectivity of this 32CA reaction, considerably. (2) The B3LYP functional overestimated and underestimated the activation barriers and the reaction exothermicities, respectively, compared to the MPWB1K and M06-2X functionals in these reactions. However, a single

point energy calculation using the MPWB1K/6-311G(d,) improves the energetic results, drastically. (3) DMSO and toluene increases the activation energies relative to gas phase in all pathways, especially in the catalyzed process through iminium intermediate that has an ionic nature. A polar DMSO solvent decreased the rate of this reaction greater than non-polar toluene solvent. (4) The piperidine organocatalyst lowers the HOMO and LUMO energy levels considerably, which increases the electrophilicity of dipolarophile in the iminium form **1I**, greatly. (5) While the catalyst-free 32CA reaction of **1** with phenyl azide **2** is an almost synchronous reaction with non-polar character, the catalyzed one is a polar and asynchronous cycloaddition that can be classified as a two-stage one-step process. (6) It seems the prediction of the regioselectivity based on Parr functions depends on the employed basis set. While, the terminal nitrogen of phenyl azide is predicted to be more nucleophilic nitrogen with standard 6-31G(d), 6-31+G(d) and 6-311G(d,p) basis sets, incorrectly, employing of larger 6-311+G(d,p) basis set predicts correctly the more nucleophilic nitrogen. (7) The present ELF topological analyses along the IRCs of both catalyzed and uncatalyzed 32CA reactions indicate that the position of the steps and the sequence change partially but the overall description remains almost constant. While the first C_1-N_1 single bond is formed as a dative bond, the formation of the second C_2-N_3 bond takes place via a C-to-N coupling between the interacting centers of the reagents, which have monosynaptic basins. The ELF analyses assert the piperidine catalyzed 32CA reaction of **1It** with phenyl azide **2** is a two-stage one-step process in which the C_2-N_3 bond is formed in the final step of the IRC, after completion of the C_1-N_1 bond formation.

Acknowledgements

The authors are thankful to the Research Council of Ferdowsi University of Mashhad, Iran (Grant no. 3/29786) for financial support. We also like to express our sincere gratitude to Professor Mohammad Izadyar for his helpful comments and reviewing the manuscript.

Supporting Information

A brief discussion about comparison of functionals and basis sets, details of ELF topological analysis, Tables S1-S8, Figures S1 and S2, Complete ref 46, absolute energies, Cartesian coordinates and geometries of stationary points at M06-2X/6-31G(d) level.

REFRENCES

1. A. Lauria, R. Delisi, F. Mingoia, A. Terenzi, A. Martorana, G. Barone and A. M. Almerico, *European Journal of Organic Chemistry*, 2014, **2014**, 3289-3306.
2. S. G. Agalave, S. R. Maujan and V. S. Pore, *Chemistry–An Asian Journal*, 2011, **6**, 2696-2718.
3. T. Efthymiou, W. Gong and J.-P. Desaulniers, *Molecules*, 2012, **17**, 12665-12703.

4. T. G. Gonzaga, D. R da Rocha, F. de C da Silva and V. F Ferreira, *Current topics in medicinal chemistry*, 2013, **13**, 2850-2865.
5. Y.-C. Duan, Y.-C. Ma, E. Zhang, X.-J. Shi, M.-M. Wang, X.-W. Ye and H.-M. Liu, *European journal of medicinal chemistry*, 2013, **62**, 11-19.
6. Y. L. Angell and K. Burgess, *Chemical Society Reviews*, 2007, **36**, 1674-1689.
7. R. Huisgen, *Angewandte Chemie International Edition in English*, 1963, **2**, 565-598.
8. R. Huisgen, *Angewandte Chemie International Edition in English*, 1963, **2**, 633-645.
9. C. W. Tornøe, C. Christensen and M. Meldal, *The Journal of organic chemistry*, 2002, **67**, 3057-3064.
10. V. V. Rostovtsev, L. G. Green, V. V. Fokin and K. B. Sharpless, *Angewandte Chemie*, 2002, **114**, 2708-2711.
11. L. Zhang, X. Chen, P. Xue, H. H. Sun, I. D. Williams, K. B. Sharpless, V. V. Fokin and G. Jia, *Journal of the American Chemical Society*, 2005, **127**, 15998-15999.
12. L. M. Gaetke and C. K. Chow, *Toxicology*, 2003, **189**, 147-163.
13. K. Jomova and M. Valko, *Toxicology*, 2011, **283**, 65-87.
14. E. M. Sletten and C. R. Bertozzi, *Angewandte Chemie International Edition*, 2009, **48**, 6974-6998.
15. N. J. Agard, J. A. Prescher and C. R. Bertozzi, *Journal of the American Chemical Society*, 2004, **126**, 15046-15047.
16. J. M. Baskin, J. A. Prescher, S. T. Laughlin, N. J. Agard, P. V. Chang, I. A. Miller, A. Lo, J. A. Codelli and C. R. Bertozzi, *Proceedings of the National Academy of Sciences*, 2007, **104**, 16793-16797.
17. S. W. Kwok, J. R. Fotsing, R. J. Fraser, V. O. Rodionov and V. V. Fokin, *Organic letters*, 2010, **12**, 4217-4219.
18. M. E. Meza-Aviña, M. K. Patel, C. B. Lee, T. J. Dietz and M. P. Croatt, *Organic letters*, 2011, **13**, 2984-2987.
19. N. Seus, B. Goldani, E. J. Lenardão, L. Savegnago, M. W. Paixão and D. Alves, *European Journal of Organic Chemistry*, 2014, **2014**, 1059-1065.
20. L. Wang, S. Peng, L. J. T. Danence, Y. Gao and J. Wang, *Chemistry–A European Journal*, 2012, **18**, 6088-6093.
21. D. B. Ramachary, K. Ramakumar and V. V. Narayana, *Chemistry–A European Journal*, 2008, **14**, 9143-9147.
22. W. Li, Z. Du, J. Huang, Q. Jia, K. Zhang and J. Wang, *Green Chemistry*, 2014, **16**, 3003-3006.
23. W. Li, X. Zhou, Y. Luan and J. Wang, *RSC Advances*, 2015, **5**, 88816-88820.
24. W. Li, Q. Jia, Z. Du and J. Wang, *Chemical Communications*, 2013, **49**, 10187-10189.
25. A. Ali, A. G. Corrêa, D. Alves, J. Zukerman-Schpector, B. Westermann, M. A. Ferreira and M. W. Paixão, *Chemical Communications*, 2014, **50**, 11926-11929.
26. C. G. Lima, A. Ali, S. S. van Berkel, B. Westermann and M. W. Paixão, *Chemical Communications*, 2015, **51**, 10784-10796.
27. S. S. Ramasastry, *Angewandte Chemie International Edition*, 2014, **53**, 14310-14312.
28. A. B. Shashank, S. Karthik, R. Madhavachary and D. B. Ramachary, *Chemistry–A European Journal*, 2014, **20**, 16877-16881.
29. Q. Jia, G. Yang, L. Chen, Z. Du, J. Wei, Y. Zhong and J. Wang, *European Journal of Organic Chemistry*, 2015, **2015**, 3435-3440.
30. J. Thomas, S. Jana, J. John, S. Liekens and W. Dehaen, *Chemical Communications*, 2016.

31. G. Cheng, X. Zeng, J. Shen, X. Wang and X. Cui, *Angewandte Chemie International Edition*, 2013, **52**, 13265-13268.
32. J. Thomas, J. John, N. Parekh and W. Dehaen, *Angewandte Chemie International Edition*, 2014, **53**, 10155-10159.
33. D. K. J. Yeung, T. Gao, J. Huang, S. Sun, H. Guo and J. Wang, *Green Chemistry*, 2013, **15**, 2384-2388.
34. D. B. Ramachary, A. B. Shashank and S. Karthik, *Angewandte Chemie International Edition*, 2014, **53**, 10420-10424.
35. L. J. T. Danence, Y. Gao, M. Li, Y. Huang and J. Wang, *Chemistry–A European Journal*, 2011, **17**, 3584-3587.
36. J. John, J. Thomas and W. Dehaen, *Chemical Communications*, 2015, **51**, 10797-10806.
37. M. Belkheira, D. El Abed, J. M. Pons and C. Bressy, *Chemistry–A European Journal*, 2011, **17**, 12917-12921.
38. W. Li and J. Wang, *Angewandte Chemie International Edition*, 2014, **53**, 14186-14190.
39. N. Seus, L. C. Goncalves, A. M. Deobald, L. Savegnago, D. Alves and M. W. Paixao, *Tetrahedron*, 2012, **68**, 10456-10463.
40. D. B. Ramachary and A. B. Shashank, *Chemistry–A European Journal*, 2013, **19**, 13175-13181.
41. W. Li, Z. Du, K. Zhang and J. Wang, *Green Chemistry*, 2015, **17**, 781-784.
42. J. Tajabadi, M. Bakavoli, M. Gholizadeh, H. Eshghi and M. Izadyar, *RSC Advances*, 2015, **5**, 38489-38498.
43. J. Tajabadi, M. Bakavoli, M. Gholizadeh, H. Eshghi and A. Khojastehnezhad, *Progress in Reaction Kinetics and Mechanism*, 2014, **39**, 233-248.
44. M. Rahimizadeh, H. Eshghi, A. Khojastehnezhad, F. Moeinpour, M. Bakavoli and J. Tajabadi, *Journal of Fluorine Chemistry*, 2014, **162**, 60-65.
45. A. Khojastehnezhad, H. Eshghi, F. Moeinpour, M. Bakavoli, M. Izadyar and J. Tajabadi, *Structural Chemistry*, 2015, 1-7.
46. Gaussian 09 (Revision A.02): M. J. Frisch et al., see Supporting Information.
47. A. D. Becke, *The Journal of chemical physics*, 1993, **98**, 5648-5652.
48. C. Lee, W. Yang and R. G. Parr, *Physical review B*, 1988, **37**, 785.
49. Y. Zhao and D. G. Truhlar, *The Journal of Physical Chemistry A*, 2004, **108**, 6908-6918.
50. Y. Zhao and D. G. Truhlar, *Theoretical Chemistry Accounts*, 2008, **120**, 215-241.
51. V. Barone and M. Cossi, *The Journal of Physical Chemistry A*, 1998, **102**, 1995-2001.
52. M. Cossi, N. Rega, G. Scalmani and V. Barone, *Journal of computational chemistry*, 2003, **24**, 669-681.
53. C. Gonzalez and H. B. Schlegel, *Journal of Physical Chemistry*, 1990, **94**, 5523-5527.
54. C. Gonzalez and H. B. Schlegel, *The Journal of chemical physics*, 1991, **95**, 5853-5860.
55. S. Noury, X. Krokidis, F. Fuster and B. Silvi, *Computers & chemistry*, 1999, **23**, 597-604.
56. Gauss View, Version 5, R. Dennington, T. Keith and J. Millam, Semichem Inc., Shawnee Mission, KS, 2009.
57. S. N. Pieniazek, F. R. Clemente and K. N. Houk, *Angewandte Chemie International Edition*, 2008, **47**, 7746-7749.
58. M. D. Wodrich, C. Corminboeuf and P. v. R. Schleyer, *Organic letters*, 2006, **8**, 3631-3634.

59. S. F. Sousa, P. A. Fernandes and M. J. Ramos, *The Journal of Physical Chemistry A*, 2007, **111**, 10439-10452.
60. I. Y. Zhang, J. Wu and X. Xu, *Chemical Communications*, 2010, **46**, 3057-3070.
61. Y. Zhao and D. G. Truhlar, *Accounts of chemical research*, 2008, **41**, 157-167.
62. E. G. Hohenstein, S. T. Chill and C. D. Sherrill, *Journal of chemical theory and computation*, 2008, **4**, 1996-2000.
63. Y. Lan, L. Zou, Y. Cao and K. Houk, *The Journal of Physical Chemistry A*, 2011, **115**, 13906-13920.
64. K. A. Nacereddine, H. Layeb, F. Chafaa, W. Yahia, A. Djerourou and L. R. Domingo *RSC Advances*, 2015, **5**, 64098-64105.
65. L. R. Domingo, M. J. Aurell, P. Pérez and R. Contreras, *Tetrahedron*, 2002, **58**, 4417-4423.
66. P. Jaramillo, L. R. Domingo, E. Chamorro and P. Pérez, *Journal of Molecular Structure: THEOCHEM*, 2008, **865**, 68-72.
67. L. R. Domingo, E. Chamorro and P. Pérez, *The Journal of organic chemistry*, 2008, **73**, 4615-4624.
68. L. R. Domingo, *RSC Advances*, 2014, **4**, 32415-32428.
69. A. E. Reed, R. B. Weinstock and F. Weinhold, *The Journal of Chemical Physics*, 1985, **83**, 735-746.
70. A. E. Reed, L. A. Curtiss and F. Weinhold, *Chemical Reviews*, 1988, **88**, 899-926.
71. L. R. Domingo and J. A. Sáez, *Organic & biomolecular chemistry*, 2009, **7**, 3576-3583.
72. L. R. Domingo, M. Arnó and J. Andrés, *The Journal of Organic Chemistry*, 1999, **64**, 5867-5875.
73. L. R. Domingo, M. J. Aurell and P. Pérez, *Organic & biomolecular chemistry*, 2014, **12**, 7581-7590.
74. L. R. Domingo, P. Pérez and J. A. Sáez, *RSC Advances*, 2013, **3**, 1486-1494.
75. P. Pérez and L. R. Domingo, *European Journal of Organic Chemistry*, 2015, **2015**, 2826-2834.
76. J. Andrés, S. Berski, L. R Domingo, V. Polo and B. Silvi, *Current Organic Chemistry*, 2011, **15**, 3566-3575.
77. L. R. Domingo, E. Chamorro and P. Pérez, *Organic & biomolecular chemistry*, 2010, **8**, 5495-5504.
78. A. D. Becke and K. E. Edgecombe, *The Journal of chemical physics*, 1990, **92**, 5397-5403.
79. A. Savin, O. Jepsen, J. Flad, O. K. Andersen, H. Preuss and H. G. von Schnering, *Angewandte Chemie International Edition in English*, 1992, **31**, 187-188.
80. B. Silvi and A. Savin, *Nature*, 1994, **371**, 683-686.
81. L. R. Domingo, E. Chamorro and P. Pérez, *Letters in Organic Chemistry*, 2010, **7**, 432-439.
82. L. R. Domingo and J. A. Saéz, *The Journal of organic chemistry*, 2011, **76**, 373-379.
83. L. R. Domingo, J. A. Saéz, R. J. Zaragozá and M. Arnó, *The Journal of organic chemistry*, 2008, **73**, 8791-8799.

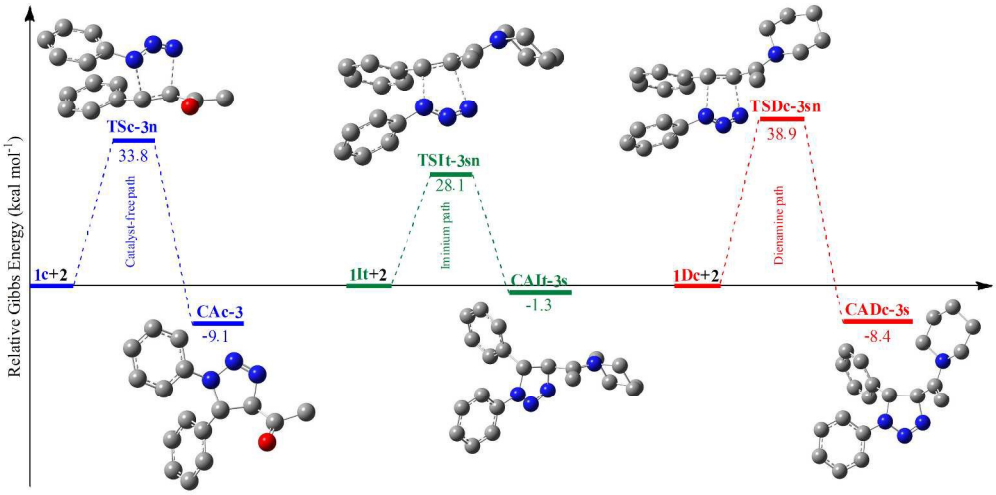

1087x533mm (96 x 96 DPI)

The mechanism of uncatalyzed and piperidine organocatalyzed cycloaddition reaction of benzalacetone with phenyl azide was investigated by computational study.